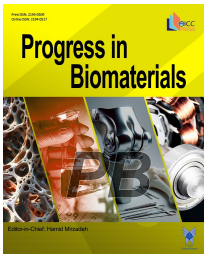

Volume 13, Issue 1, 132402 (1-16)

Progress in Biomaterials (PIBM)

https://doi.org/10.57647/pibm.2024.132402

Development and Characterization of ZnO-Loaded Solid Lipid Nanoparticles for Oral Delivery: Physicochemical, Cytocompatibility, and Antibacterial Evaluation

Zahra Inanloo[1], Mohammad Yousefi[2,*], Sahar Baniyaghoob[1]

Department of Chemistry, SR.C., Islamic Azad University, Tehran, Iran.
Department of Chemistry, TeMS.C., Islamic Azad University, Tehran, Iran.

[*]**Corresponding author:** myousefi50@iau.ac.ir

Original Research

Received:
11 June 2023
Revised:
18 October 2023
Accepted:
25 November 2023
Published online:
30 March 2024

Abstract:

Chitosan-coated solid lipid nanoparticles loaded with zinc oxide (ZnO-CS-SLNs) were developed to enhance oral zinc delivery and improve formulation performance. The nanoparticles were synthesized via a microemulsion technique and exhibited spherical morphology, an average diameter of 91.2 ± 2.8 nm, a positive zeta potential (+25 mV), and high encapsulation efficiency ($90 \pm 3\%$), quantified using ICP-OES. FTIR, DSC, and XRD analyses confirmed structural integrity and uniform ZnO distribution within the lipid matrix. FE-SEM and TEM imaging revealed homogeneous particles with no signs of aggregation.

In vitro release studies conducted in simulated gastric (pH 1.2) and intestinal (pH 6.8) fluids demonstrated sustained release profiles reaching up to 93% over 24 hours, consistent with Higuchi kinetics. Cytotoxicity assays on AGS cells indicated excellent biocompatibility, with cell viability exceeding 100% across all tested concentrations. Antibacterial activity of ZnO-002 was validated against Gram-positive and Gram-negative strains using disk diffusion, MIC, and MBC assays. Accelerated stability testing over six months (40 ± 2 °C, $75 \pm 5\%$ RH) confirmed the physical and colloidal stability of the formulations. Collectively, these results support ZnO-CS-SLNs as a robust oral delivery system with multifunctional attributes and consistent in vitro performance.

Keywords: Zinc oxide; Solid lipid nanoparticles; Chitosan; Oral delivery; Bioavailability; Antimicrobial activity; Cytocompatibility; Sustained release

Cite this article: Inanloo, Z., Yousefi, M., Baniyaghoob, S. Development and Characterization of ZnO-Loaded Solid Lipid Nanoparticles for Oral Delivery: Physicochemical, Cytocompatibility, and Antibacterial Evaluation. *Progress in Biomaterials* **13**(1), Article 02 (2024).

1. Introduction

Zinc is an essential trace element involved in a wide array of biological processes, including enzymatic catalysis, gene regulation, immune function, antioxidant defence, and tissue repair. It is the second most abundant trace metal in the human body after iron, present in all organs and tissues Prasad, 2008; King, 2011. Despite its critical role, zinc deficiency remains one of the most prevalent micronutrient deficiencies worldwide, affecting approximately two billion people-particularly in low-income regions with limited access to zinc-rich foods Black, 2003; Brown et al., 2001. This deficiency is associated with impaired growth, weakened immunity, delayed wound healing, and increased susceptibility to infections, especially in children Trivedi et al., 2009. Zinc oxide (ZnO) is widely used in supplementation due to its high elemental zinc content ($\sim 80\%$), chemical stability, affordability, and potent antimicrobial properties Mishra et al., 2017; Allen et al., 2006. However, its clinical utility for oral administration is limited by poor aqueous solubility, low gastrointestinal absorption, metallic taste, and potential for gastric irritation Allen et al., 2006; Salgueiro et al., 2002. These drawbacks reduce patient compliance and therapeutic efficacy, particularly during long-term use. Among the various zinc salts used for supplementation, such as zinc sulfate, acetate, gluconate, and oxide, zinc oxide (ZnO) has attracted considerable interest due to its high elemental zinc content ($\sim 80\%$), chemical stability, affordability, and potent antimicrobial properties Mishra

et al., 2017. ZnO has been widely employed not only as a dietary supplement but also in cosmetics, sunscreens, and wound dressings due to its broad-spectrum antimicrobial and anti-inflammatory properties. However, the clinical utility of ZnO in oral supplementation is limited by its poor aqueous solubility, which restricts dissolution in gastrointestinal fluids and leads to low oral bioavailability Allen et al., 2006. Moreover, ZnO's metallic taste and potential to cause gastrointestinal irritation (e.g., nausea, abdominal pain) pose challenges to patient adherence, particularly during long-term use Salgueiro et al., 2002.

To address these limitations, nanotechnology-based delivery systems have emerged as promising alternatives. Among them, solid lipid nanoparticles (SLNs) offer several advantages for oral drug delivery, including enhanced solubility of poorly water-soluble compounds, protection from enzymatic degradation, and controlled release Mehnert and Mäder, 2001; Ekambaram et al., 2012; Mahajan et al., 2015. SLNs are composed of biocompatible lipids that remain solid at body temperature and can be stabilized using surfactants or polymers Müller et al., 2002.

In this study, we developed a novel oral zinc delivery system by encapsulating ZnO within SLNs and coating the nanoparticles with chitosan-a natural, biodegradable, and mucoadhesive polymer. Chitosan enhances gastrointestinal retention and absorption by interacting with negatively charged mucosal surfaces Bernkop-Schnürch and Dünnhaupt, 2012; Mohammed et al., 2017. Additionally, it contributes antimicrobial and anti-inflammatory properties, further boosting the therapeutic potential of the formulation Hosseini et al., 2020. Unlike previous studies that primarily focused on topical or cosmetic applications of ZnO nanoparticles Raghupathi et al., 2011; Pignatello et al., 2018, our research introduces a dual-functional oral formulation with both nutritional and antimicrobial benefits. The specific problem addressed is the poor bioavailability and gastrointestinal side effects of conventional ZnO supplements. By encapsulating ZnO in chitosan-coated SLNs, we aim to improve solubility, enhance mucosal absorption, reduce irritation, and provide sustained zinc release.

The novelty of this work lies in the integration of physicochemical characterisation, cytocompatibility testing, and microbiological evaluation to validate the formulation's safety, efficacy, and scalability. This comprehensive approach positions ZnO-CS-SLNs as a promising alternative to traditional zinc supplements, particularly for vulnerable populations such as children and patients with compromised immunitcussy. Recent studies have highlighted the oral safety and biocompatibility of ZnO-based nanocarriers and solid lipid nanoparticles, supporting their potential for gastrointestinal delivery Scioli-Montoto et al., 2020; PubChem, 2024.

2. Material and methods

2.1 Materials

The following materials were used in this study, all of which were of analytical grade and used without further purification unless otherwise stated:

Stearic acid (purity $\geq$ 98%, CAS No. 57-11-4) was purchased from Merck (Germany) and served as the lipid core for SLN formulation, Chitosan (high molecular weight, degree of deacetylation $\geq$ 85%, CAS No. 9012-76-4) was obtained from Sigma-Aldrich (Germany) and used as a coating polymer to enhance mucoadhesion and stability, Zinc oxide (ZnO) (purity $\geq$ 99%, nanopowder, particle size $<$ 100 nm, CAS No. 1314-13-2) was sourced from Merck (Germany) and used as the active ingredient for encapsulation, Egg lecithin (purity $\geq$ 98%, CAS No. 8002-43-5) was purchased from Merck and used as a natural emulsifier to stabilize the lipid phase, Tween 20 (polyoxyethylene sorbitan monolaurate, purity $\geq$ 99%, CAS No. 9005-64-5) was used as the primary surfactant in the microemulsion system, n-Butanol (HPLC grade, purity $\geq$ 99.5%, CAS No. 71-36-3) was used as a co-surfactant to enhance emulsification efficiency, Mannitol (purity $\geq$ 99%, CAS No. 69-65-8) was used as a cryoprotectant during freeze-drying to preserve nanoparticle integrity, Distilled water was freshly prepared in the laboratory and used throughout the formulation and characterization processes. n-Butanol was used at a trace concentration as a co-surfactant. According to PubChem (CID: 263) and PubMed toxicological data (PMID: 18830864), the oral LD_{50} in rats ranges from 790 to 4,360 mg/kg, which is far above the levels applied here. In addition, n-butanol is listed in the FDA Inactive Ingredients Database (IID) and historically recognized as a food flavouring agent, confirming its low oral toxicity at trace levels Program, 2008; Food and (FDA), 2024; Date et al., 2016.

2.2 Preparation of zinc oxide-loaded solid lipid nanoparticles (ZnO-SLNs)

Zinc oxide-loaded solid lipid nanoparticles (ZnO-SLNs) were prepared using a modified hot microemulsion technique followed by ultrasonication and chitosan coating. The method was optimized to ensure uniform particle size, high encapsulation efficiency, and reproducibility.

Lipid Phase Preparation: Stearic acid (0.7 mM) and egg lecithin (0.2 mM) were accurately weighed and melted at 70 $\pm$ 2 °C under continuous magnetic stirring (1200 rpm) to form the lipid phase. Zinc oxide (ZnO) was added to the molten lipid in two concentrations-0.15 mM and 0.3 mM-based on preliminary solubility and cytocompatibility studies. The mixture was probe-sonicated (30% amplitude, 2 min, pulse on/off) to ensure homogeneous dispersion of ZnO within the lipid matrix.

Aqueous Phase Preparation: Separately, Tween 20 (0.4 mM) and n-butanol (1.639 mM) were dissolved in distilled water and preheated to match the lipid phase temperature. This surfactant system was selected for its proven emulsification efficiency and compatibility with oral formulations. The aqueous phase was also probe-sonicated (30% amplitude, 2 min) to enhance dispersion.

Microemulsion formation: The hot aqueous phase was gradually added to the lipid phase under constant stirring, maintaining a temperature of 67 $\pm$ 2 °C. The resulting emulsion was subjected to a second round of ultrasonication (30% amplitude, 2 min) to reduce droplet size and promote uniformity. Based on the formulation components and previous reports, the pH of the resulting microemulsion was estimated to be mildly acidic, ranging between 5.5 and 6.5,

which is favourable for nanoparticle stability and prevents aggregation during synthesis.
Nanoparticle solidification: The hot emulsion was immediately poured into cold distilled water (4 ± 1 °C) in a 1:10 volume ratio under gentle stirring. This thermal shock induced rapid solidification of lipid droplets, forming a milky suspension of ZnO-SLNs.
Chitosan coating: To enhance mucoadhesion and stability, a 0.1% (w/v) chitosan solution (prepared in 1% acetic acid) was added dropwise to the nanoparticle suspension under mild stirring. The positively charged chitosan electrostatically interacted with the negatively charged SLNs, forming a uniform coating layer.
Cryoprotection and freeze-drying: Mannitol (5% w/v) was added as a cryoprotectant to prevent aggregation during the lyophilisation process. The final dispersion was freeze-dried overnight at −40 °C to obtain a dry powder suitable for storage and further characterisation.
The resulting formulations were designated as ZnO-001 (0.15 mM ZnO) and ZnO-002 (0.3 mM ZnO) and were used throughout the study for physicochemical, cytocompatibility, and antimicrobial evaluations.

2.3 Characterisation methods

2.3.1 Particle size, polydispersity index (PDI), and zeta potential

The hydrodynamic diameter, polydispersity index (PDI), and zeta potential of the SLNs were determined using a Malvern Zetasizer Nano ZS (UK). Samples were analyzed before and after freeze-drying, in triplicate, at room temperature to assess colloidal stability Bernkop-Schnürch and Dünnhaupt, 2012.

2.3.2 Fourier Transform Infrared (FTIR) spectroscopy

FT-IR spectroscopy was performed using a Shimadzu FT-IR-8300 E (Japan) to analyze potential interactions among formulation components. Spectra of ZnO, stearic acid, chitosan, and the final formulation were recorded between 4000 and 400 cm^{-1} using KBr disks as a reference.

2.3.3 Differential Scanning Calorimetry (DSC)

Thermal behaviour and phase transitions of the nanoparticles and individual ingredients were studied using a DSC STA6000 (PerkinElmer, USA). Approximately 10 mg of each sample was sealed in aluminum pans and heated from 40 to 300 °C at a rate of 10 °C/min under nitrogen flow (10 mL/min). This analysis helped confirm ZnO dispersion and lipid crystallinity.

2.3.4 X-ray Diffraction (XRD) analysis

XRD was conducted to evaluate the crystalline or amorphous nature of ZnO-SLNs using an Xpert Pro Panalytical diffractometer (Netherlands). Measurements were performed at 40 kV and 40 mA using Cu-Kα radiation over a 2θ range of 5°–80°. The diffraction patterns were compared with standard ZnO peaks to confirm structural integrity.

2.3.5 Morphological analysis (FE-SEM and TEM)

Surface morphology was examined using field emission scanning electron microscopy (FE-SEM, Zeiss SIGMA VP-FESEM, Germany). Samples were mounted on aluminium stubs, dried, and sputter-coated with gold. Internal structure and particle dispersion were visualized using transmission electron microscopy (TEM, Philips EM208S, Netherlands) after negative staining with 2% phosphotungstic acid Raghupathi et al., 2011; Pignatello et al., 2018.

2.3.6 Thermogravimetric analysis (TGA)

Thermogravimetric analysis (TGA) was performed to investigate the thermal behaviour and stability of ZnO-SLNs. Approximately 5 – 30 mg of each lyophilized sample (ZnO-001 and ZnO-002) was placed in an aluminium pan and analysed using a Shimadzu TGA-50H thermal gravimetric analyser. The samples were heated from 25 to 400 °C at a constant heating rate of 10 °C/min under a nitrogen atmosphere (30 mL/min). The percentage of weight loss was recorded as a function of temperature, and the decomposition steps corresponding to the organic components (lipids, surfactants, and chitosan) and the residual fraction (ZnO) were determined. This method has been widely applied for studying thermal stability and inorganic content in nanoparticle-based systems Winter et al., 2016; Gasco, 1997.

2.3.7 Drug loading and encapsulation efficiency

Encapsulation efficiency (EE%) and drug loading (DL%) were determined by ultrafiltration using Amicon Ultra-15 centrifugal filters (100 kDa). SLN dispersions were centrifuged at 21,000 rcf for 30 minutes at 4 °C. The concentration of unencapsulated ZnO in the filtrate was quantified using inductively coupled plasma optical emission spectroscopy (ICP-OES, PerkinElmer Optima 8000). EE% and DL% were calculated using standard equations Convention, 2019. Considering the inorganic nature of ZnO and its limited solubility in conventional solvents, ICP-OES was selected as the most appropriate and reliable method for quantifying zinc content and calculating encapsulation efficiency. Alternative methods such as UV-Vis or HPLC were deemed unsuitable for this compound due to matrix interference and solubility constraints.

2.3.8 *In vitro* drug release profile

The *in vitro* release of zinc from ZnO-SLNs was investigated using the dialysis bag diffusion technique. Approximately 5 mL of each sample was placed into dialysis tubing (MWCO 12–14 kDa) and immersed in 500 mL of release medium maintained at 37 ± 0.5 °C. Two different media were used to simulate gastrointestinal conditions:

- Simulated gastric fluid: 0.1 N HCl, pH 1.2.
- Simulated intestinal fluid: phosphate buffer, pH 6.8.

The release medium was stirred continuously at 75 rpm using a USP paddle apparatus (Erweka DT 720, Germany). Aliquots (2 mL) were withdrawn at predetermined intervals (0.5, 1, 2, 4, 6, 8, 12, and 24 hours) and replaced with an equal volume of fresh medium to maintain sink conditions. Zinc concentration in the samples was quantified using inductively coupled plasma optical emission spectrometry

(ICP-OES), and cumulative release (%) was calculated accordingly Convention, 2019.

2.3.9 Cytotoxicity evaluation (MTT assay)

The cytotoxic potential of ZnO-SLNs was assessed on human gastric adenocarcinoma cells (AGS) using the MTT assay. Cells were seeded in 96-well plates at a density of 1×10^4 cells/well and incubated overnight. SLN formulations were applied at concentrations ranging from 15.625 to 500 µg/mL for 24 and 48 hours. Following treatment, cells were incubated with MTT reagent (0.5 mg/mL) for 3 hours. The resulting formazan crystals were solubilized in DMSO, and absorbance was measured at 570 nm with a reference wavelength of 630 nm using a microplate reader. Cell viability (%) was calculated relative to untreated controls Clinical and Institute, 2015.

2.3.10 Antimicrobial activity assessment

Antimicrobial efficacy of the optimized ZnO-002 SLN was evaluated against *E. coli* (ATCC 25922) and *S. aureus* (ATCC 6538) using disc diffusion and broth microdilution methods, following CLSI M07-A10 guidelines Müller et al., 2000. Sterile discs loaded with SLNs were placed on Mueller-Hinton agar plates inoculated with standardized bacterial suspensions (0.5 McFarland). After incubation (24 h, 37 °C), inhibition zones were recorded. For MIC and MBC determination, two-fold serial dilutions of SLNs were prepared in 96-well plates, with MIC defined as the lowest concentration preventing visible growth and MBC as the lowest concentration causing $\geq$ 99.9% killing. All assays were performed in triplicate, and results are expressed as mean $\pm$ SD. Statistical significance was determined by one-way ANOVA followed by Tukey's post hoc test ($p < 0.05$).

2.3.11 Accelerated stability testing

Stability of the optimized ZnO-SLN formulation was assessed under accelerated conditions (40 $\pm$ 2 °C, 75 $\pm$ 5% RH) over 6 months. Samples were stored in opaque polyethylene containers to prevent light-induced degradation. At 0, 3, and 6 months, formulations were analyzed for particle size, zeta potential, and encapsulation efficiency (EE%) to monitor physicochemical stability. All measurements were performed in triplicate using validated analytical methods Convention, 2019.

3. Result and discussion

3.1 Characterization of particle size, polydispersity, and surface charge

To evaluate the physicochemical properties of the synthesised ZnO-SLN formulations, particle size, polydispersity index (PDI), and zeta potential were measured both before and after lyophilisation. These parameters are critical for predicting colloidal stability, cellular uptake, and *in vivo* performance of lipid-based nanocarriers.

Uncoated SLNs exhibited an average particle size of 141.1 $\pm$ 2.1 nm, which slightly decreased to 136.5 $\pm$ 3.4 nm after lyophilization. Incorporation of ZnO reduced the particle size marginally (ZnO-001: 132.2 $\pm$ 1.3 nm; ZnO-002: 131.87 $\pm$ 2.7 nm), likely due to ZnO–lipid matrix interactions that promote tighter packing. Upon chitosan coating, the particle size further decreased, especially after lyophilization (ZnO-001: 99.4 $\pm$ 3.5 nm; ZnO-002: 91.2 $\pm$ 2.8 nm), indicating enhanced structural compaction and cryoprotective stabilization.PDI values ranged from 0.525 to 0.625, suggesting moderate polydispersity and acceptable homogeneity for nanoparticle formulations. Although ZnO loading slightly increased PDI, all values remained within the acceptable range (< 0.7), indicating stable dispersion.

Zeta potential measurements revealed a shift from negative values in uncoated SLNs (-15 to -24.2 mV) to positive values after chitosan coating ($+28.4$ to $+32.1$ mV). This surface charge reversal enhances electrostatic repulsion, improves colloidal stability, and facilitates interaction with negatively charged mucosal surfaces, potentially improving gastrointestinal uptake.

These findings are consistent with previous reports on chitosan-coated lipid nanoparticles, where surface charge modulation and size control are key determinants of biological performance and oral bioavailability Agnihotri et al., 2004; Luo et al., 2015; Joseph et al., 2016.

In addition to particle size, PDI, and zeta potential, stability data of the coated nanoparticles after lyophilization were also evaluated to demonstrate better the effect of coating and freeze-drying on the formulations (Table 1).

3.2 FTIR spectral interpretation of ZnO-loaded solid lipid nanoparticles

Fourier-transform infrared (FTIR) spectroscopy was utilized to characterize the chemical structure and investigate

Table 1. Particle size, polydispersity index (PDI), and zeta potential of ZnO–SLN formulations: uncoated, coated before lyophilization, and coated after lyophilization (n = 3, mean $\pm$ SD).

Formulation	Size (nm)	PDI	Zeta Potential (mV)
SLN (uncoated)	141.11 $\pm$ 2.1	0.540 $\pm$ 0.15	-15 $\pm$ 2.12
SLN (uncoated, after lyophilization)	136.5 $\pm$3.4	0.535 $\pm$ 0.05	-22.2$\pm$ 4.04
ZnO-001(uncoated)	132.2$\pm$1.3	0.561$\pm$0.18	-18.7$\pm$7.07
ZnO-002(uncoated)	131.87$\pm$2.7	0.625$\pm$ 0.12	-24.2$\pm$7.76
ZnO-001 (coated, before lyophilization)	130.24$\pm$ 3.3	0.525 $\pm$ 0.11	12.6 $\pm$ 5.9
ZnO-001 (coated, after lyophilization)	99.4 $\pm$ 3.5	0.545 $\pm$ 0.15	+28.4 $\pm$ 7.07
ZnO-002(coated, before lyophilization)	128.5 $\pm$ 1.1	0.565 $\pm$ 0.2	+18.4 $\pm$ 6.8
ZnO-002 (coated, after lyophilization)	91.2 $\pm$ 2.8	0.582 $\pm$ 0.15	+32.1 $\pm$ 7.76

PDI: Polydispersity index; SLN: Solid lipid nanoparticle; Zn: Zinc; SD: Standard deviation.
The values are expressed as means $\pm$ SDs (n = 3).

potential interactions among the constituents of ZnO-loaded solid lipid nanoparticles (SLNs), formulated with stearic acid, zinc oxide, Tween 20, n-butanol, chitosan, and mannitol. The FTIR spectra were analyzed to assign characteristic absorption bands and to evaluate the integrity and compatibility of the formulation components Agnihotri et al., 2004. The main absorption bands observed in the FTIR spectrum and their assignments are summarized in Table 2, and the Fourier transform infrared spectroscopy (FT-IR) is shown in Fig. 1.

3.2.1 Discussion of intermolecular interactions

Stearic Acid (Lipid Matrix): The strong C–H stretching (2920–2850 cm^{-1}) and C=O stretching (1730–1700 cm^{-1}) bands confirm the integrity of the lipid matrix. Any shift in the C=O band compared to pure stearic acid suggests potential hydrogen bonding or electrostatic interactions with chitosan or ZnO Agnihotri et al., 2004.

ZnO Nanoparticles: The presence of a distinct absorption band in the 600–400 cm^{-1} region is assigned to Zn–O stretching, confirming the successful incorporation of ZnO nanoparticles within the SLN structureJoseph et al., 2016.

Chitosan Coating: The broad O–H and N–H stretching bands (3400–3200 cm^{-1}), along with amide I and II bands (1650–1550 cm^{-1}), indicate the presence of chitosan on the nanoparticle surface. The broadening and possible intensity reduction of these bands may reflect hydrogen bonding between chitosan, stearic acid, and mannitolEspitia et al., 2012.

Tween 20 and n-Butanol: The ether (C–O–C) and alcohol (O–H) stretching bands (1150–1050 cm^{-1}) are indicative of Tween 20 and n-butanol, confirming their role as surfactant and co-surfactant, respectively.

Mannitol (Cryoprotectant): The O–H stretching region overlaps with chitosan and is consistent with the presence of polyols, supporting the role of mannitol in protecting the nanoparticles during lyophilization.

FTIR analysis provides clear evidence for the successful assembly of ZnO-loaded SLNs, with all major components identifiable by their characteristic absorption bands. The observed shifts and broadening of certain bands suggest molecular interactions, particularly hydrogen bonding, be-

Table 2. FTIR band assignments for ZnO-SLN formulation.

Observed band (cm^{-1})	Functional group / Vibration	Component(s)	Interpretation
3400–3200	O–H, N–H stretching	Chitosan, Mannitol, n-Butanol	Broad band indicating hydrogen bonding and presence of polysaccharides and polyols 1
2920–2850	C–H stretching (aliphatic)	Stearic acid, Tween 20	Confirms the presence of long-chain fatty acids and surfactant 1
1730–1700	C=O stretching (carboxylic acid)	Stearic acid	Characteristic of the lipid matrix; shifts may indicate interactions 1
1650–1550	Amide I & II (C=O, N–H bending)	Chitosan	Confirms presence of chitosan and possible amide linkages
1460–1370	CH_2/CH_3 bending	Stearic acid, Tween 20	Supports the presence of aliphatic chains 1
1150–1050	C–O–C stretching (ether, alcohol)	Tween 20, Mannitol	Indicates polyol and surfactant ether linkages 1
1050–1020	C–N stretching	Chitosan	Confirms the polysaccharide structure of chitosan
600–400	Zn–O stretching	ZnO	Signature of ZnO nanoparticles embedded in the matrix

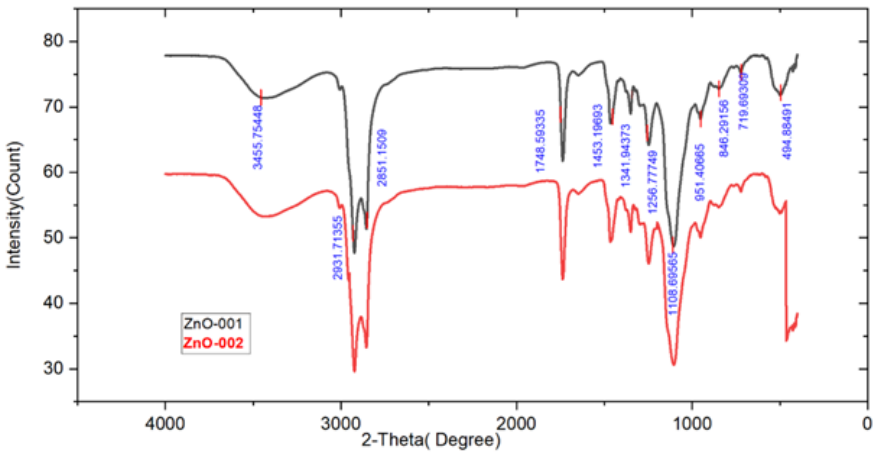

Figure 1. FT-IR spectra of ZnO-001 (black) ZnO-002(red) (FT-IR: Fourier transform infrared spectroscopy).

tween chitosan, stearic acid, and mannitol. The integrity of the ZnO nanoparticles is preserved within the lipid matrix, as indicated by the Zn–O stretching band. These findings confirm the structural stability and compositional integrity of the SLN formulation, supporting its potential for biomedical applications Ebrahimi et al., 2015.

3.3 Differential scanning calorimetry (DSC)

Differential scanning calorimetry (DSC) was employed to investigate the thermal behaviour and structural integrity of stearic acid-based solid lipid nanoparticles (SLNs) loaded with zinc oxide (ZnO). Thermograms of the lyophilized formulations are presented in figure 2. Each sample exhibited a distinct endothermic peak at approximately 69.3 °C, corresponding to the melting point of stearic acid. This consistent thermal event across all formulations confirms the preservation of the lipid's crystalline structure following nanoparticle synthesis and ZnO incorporation Yanti and Maryanti, 2021.

Notably, no thermal transitions were observed near the melting point of ZnO (1979 °C), which lies beyond the detection range of DSC instrumentation and is typically undetectable in nanoparticulate systems. The absence of ZnO-specific peaks suggests that ZnO is not present as a separate crystalline phase but is instead molecularly dispersed or exists in an amorphous state within the lipid matrix. This interpretation is further supported by the lack of secondary transitions, peak broadening, or exothermic events that would indicate phase separation, recrystallization, or polymorphic transformations Patel et al., 2014.

The similarity in thermal profiles among the formulations indicates a reproducible loading process and uniform matrix composition. The presence of a sharp, undistorted melting peak implies that ZnO incorporation did not disrupt the lipid's crystalline arrangement. Furthermore, the absence of ZnO-related transitions suggests that the nanoparticles do not contain free or crystalline ZnO, but rather that the compound is embedded in a dispersed or amorphous form. Such an arrangement is advantageous for controlled-release applications, as it facilitates gradual ion release and minimizes burst effects Yanti and Maryanti, 2021; Patel et al., 2014.

Overall, these findings confirm the successful encapsulation of ZnO within SLNs, with preserved lipid crystallinity and potential for sustained zinc ion release. The thermal stability and uniformity of the formulations underscore their suitability for oral drug delivery systems, where matrix integrity and controlled release are critical.

3.4 X-ray diffraction (XRD) analysis

The X-ray diffraction (XRD) patterns of ZnO-001 and ZnO-002 exhibit distinct diffraction peaks at 2θ values of 31.7°, 34.4°, and 36.2°, corresponding to the (100), (002), and (101) planes of hexagonal wurtzite ZnO (JCPDS No. 36-1451) Yanti and Maryanti, 2021. These peaks are characteristic of ZnO. The absence of secondary phases such as $Zn(OH)_2$ or $Zn(OH)_2CO_3$ confirms the high purity of the synthesised nanoparticles Moezzi et al., 2012.

ZnO-002 displays higher peak intensities compared to ZnO-001, suggesting improved crystallinity or larger crystallite sizes, likely due to optimized synthesis conditions Espitia et al., 2012. In contrast, the XRD pattern of the chitosan-coated SLN formulations (ZnO-CS-SLNs) reveals significantly broadened and less intense peaks, indicative of reduced crystallinity and the predominantly amorphous nature of the lipid matrix Prokhorov et al., 2020.

Importantly, this shift from sharp crystalline peaks in pure ZnO samples to broad amorphous features in SLN-Zn-Chitosan formulations highlights the structural transformation resulting from encapsulation. The lipid environment appears to suppress long-range order, leading to molecular dispersion or partial amorphisation of ZnO within the SLNs.

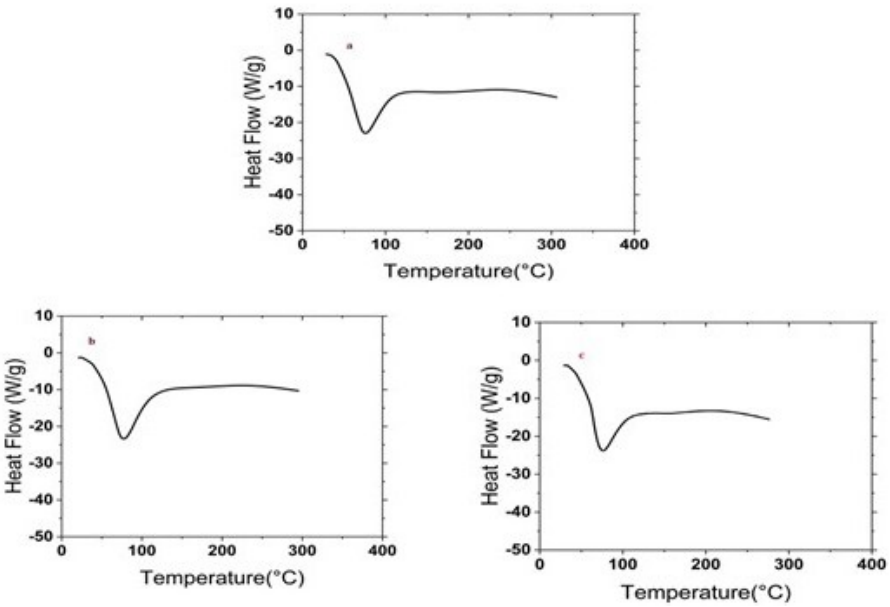

Figure 2. DSC thermograms of SLNs: (a) SLN (b) ZnO-001 (c) ZnO-002 (DSC: Differential scanning calorimetry; SLN: Solid lipid nanoparticle).

This encapsulation-induced change is consistent with the intended design of the delivery system, promoting controlled release and enhancing bioavailability. Figure 3 shows the XRD patterns of the formulations.

3.5 Morphological studies (FE-SEM and TEM)

3.5.1 FE-SEM

Field-emission scanning electron microscopy (FE-SEM) analysis demonstrated that the nanoparticles were uniformly dispersed, exhibiting a size range of 56–104 nm with a spherical shape and smooth surface texture, indicative of effective stabilization mechanisms. As shown in Fig. 4, the observed narrow size distribution is reflective of well-controlled synthesis conditions, while the absence of significant aggregation further confirms robust colloidal stability. Such physicochemical attributes are considered highly advantageous for drug delivery systems, as they facilitate:

- Enhanced cellular uptake due to optimal particle size and morphology.
- Prolonged systemic circulation, attributed to reduced aggregation and uniform surface characteristics.
- Controlled drug release profiles, enabled by the stable and consistent nanoparticle structure.

Collectively, the physical stability and morphological uniformity observed in these formulations underscore their suitability for advanced therapeutic applications.

- Compatibility with filter sterilization, ensuring sterility without compromising nanoparticle integrity.
- Excellent redispersibility, allowing for consistent dosing and ease of formulation handling.
- High drug-loading capacity, supporting efficient therapeutic payload delivery.

These findings highlight the potential of the developed nanoparticles as promising candidates for drug delivery, combining favorable physical properties with functional versatility Selvaraj et al., 2020; Patel et al., 2020; Vigani et al., 2021.

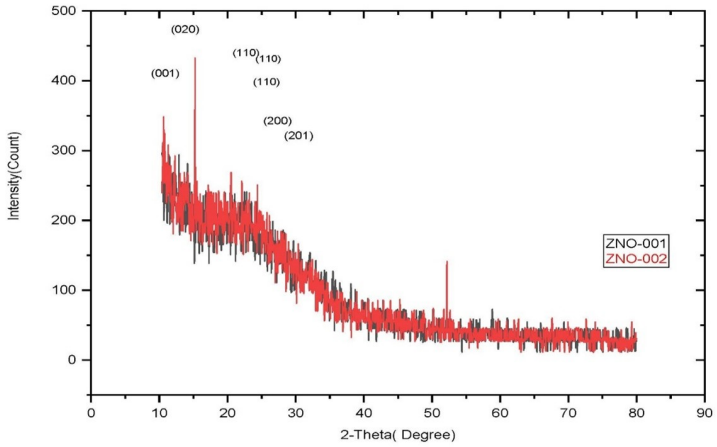

Figure 3. XRD patterns of the ZnO-001(black), ZnO-002 (red) (XRD: X-ray diffraction).

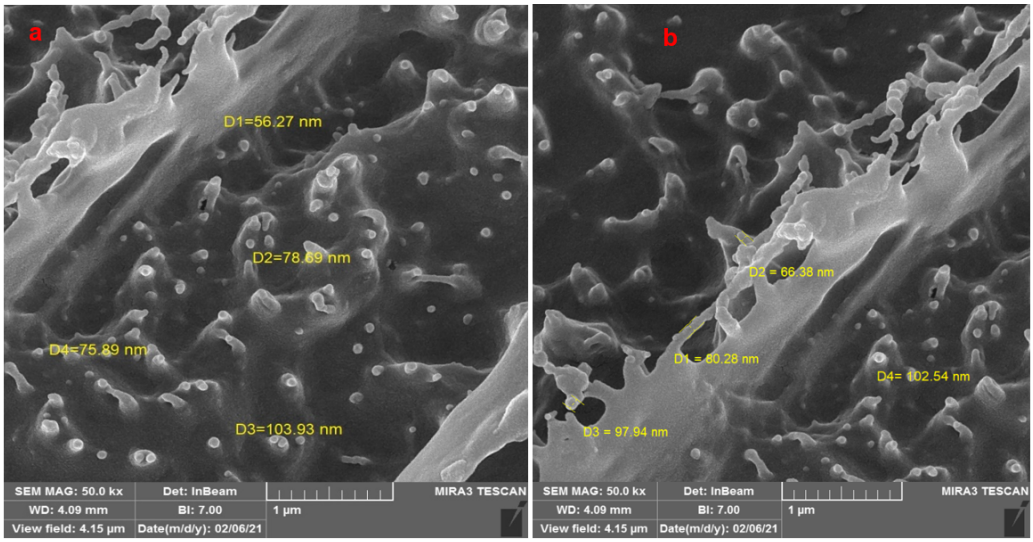

Figure 4. FE-SEM images of (a) ZnO-001, (b) ZnO-002 (FE-SEM: Field emission scanning electron microscopy).

3.5.2 TEM analysis

Summary of ZnO-Loaded Solid Lipid Nanoparticles Prepared by Microemulsion Method

Transmission electron microscopy (TEM) images of solid lipid nanoparticles (SLNs) containing zinc oxide (ZnO), synthesized via the microemulsion technique, demonstrate well-defined spherical morphology with uniform size distribution. As illustrated in Fig. 5, the ZnO nanoparticles exhibit sizes predominantly in the 18–38 nm range, embedded within lipid matrices forming core-shell structures, as indicated by contrast differences in TEM images Selvaraj et al., 2020; Patel et al., 2020; Vigani et al., 2021.

The microemulsion method effectively controls particle size and prevents aggregation, yielding SLNs typically below 100 nm, favorable for enhanced cellular uptake and biomedical applications Mehnert and Mäder, 2001. The observed homogeneity and stability of the nanoparticles suggest successful incorporation of ZnO within the lipid matrix, which is critical for improving biocompatibility and reducing cytotoxicity Müller et al., 2002.

Overall, the TEM results confirm that the microemulsion approach produces monodisperse, structurally stable ZnO-loaded SLNs suitable for drug delivery systems and other biomedical uses.

3.6 Thermogravimetric analysis (TGA)

Thermogravimetric analysis (TGA) confirmed that both ZnO-001 and ZnO-002 exhibited favorable thermal stability, supporting the successful incorporation of ZnO within the lipid matrix. ZnO-001 showed a major weight loss of approximately 79% between 109 and 143 °C, whereas ZnO-002 displayed a lower weight loss (∼ 69%) over a comparable temperature range (100–144 °C), resulting in a higher residual mass. These findings demonstrate that both formulations are thermally stable, yet ZnO-002 offers enhanced stability and stronger ZnO–lipid interactions. Similar results have been reported for chitosan-coated SLNs, where the polymer shell improves encapsulation efficiency and thermal resistance Mehnert and Mäder, 2001; Pignatello et al., 2018. Collectively, these outcomes indicate that while both systems are suitable, ZnO-002 provides superior overall performance.

Collectively, these results—supported by ICP-OES quantification and morphological analyses—provide strong evidence for the successful encapsulation of ZnO within the SLN system. The corresponding thermograms are presented in Fig. 6 (6a,6b).

3.7 *In vitro* drug release of Zinc-loaded solid lipid nanoparticles

The *in vitro* drug release profiles of ZnO-001 and ZnO-002 solid lipid nanoparticles (SLNs) were investigated under simulated gastric (pH 1.2) and intestinal (pH 6.8) conditions. As presented in figure 7 and 8 and detailed in Table 3, both formulations demonstrated a sustained release pattern over 24 h, with cumulative release reaching approximately 80% and 85% under gastric conditions, and 88% and 93% under intestinal conditions, for ZnO-001 and ZnO-002, respectively.

Before the release experiments, the dialysis membrane was validated using blank medium, confirming that no Zn^{2+} leakage occurred through the membrane. This ensures that the observed release profiles originated solely from Zn^{2+} ions diffusing from the nanoparticles. Moreover, as ICP-

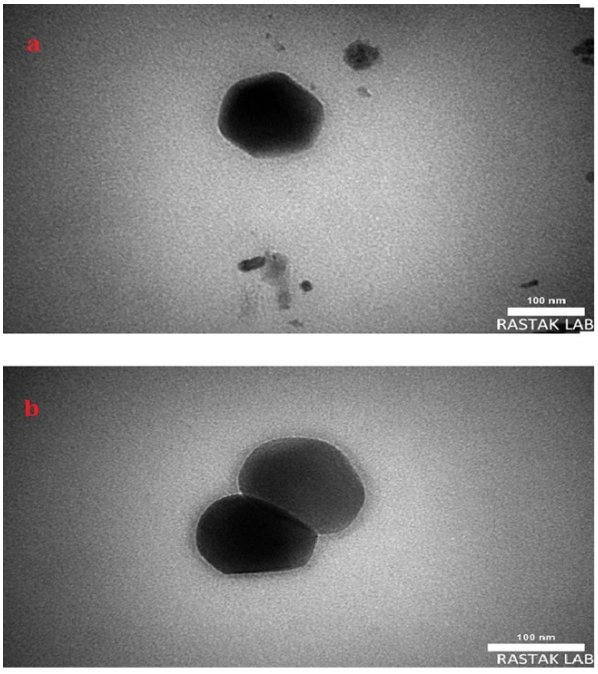

Figure 5. TEM images of (a) ZnO-001, (b) ZnO-002 (TEM: Transmission Electron Microscopy).

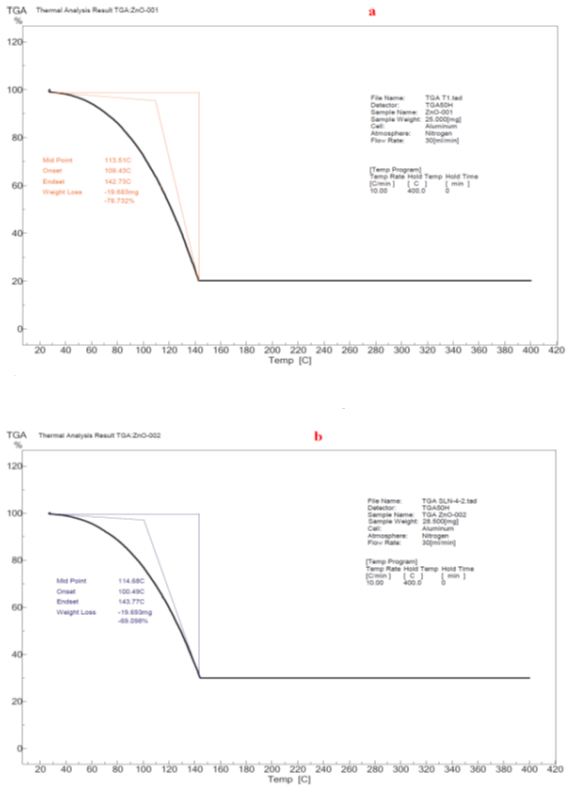

Figure 6. Thermogravimetric analysis (TGA) profile of (a) ZnO-001, (b) ZnO-002, solid lipid nanoparticles.

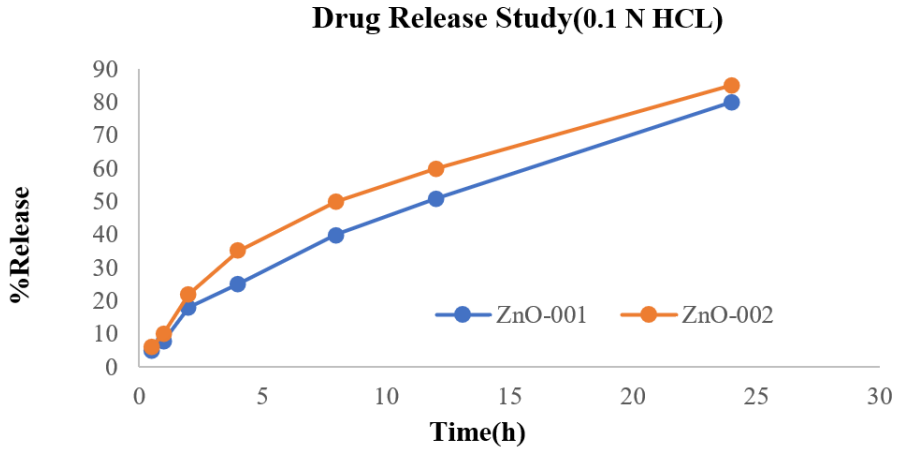

Figure 7. *In vitro* release profile study of Zn-loaded SLNs in 0.1 N HCl, pH 1.2.

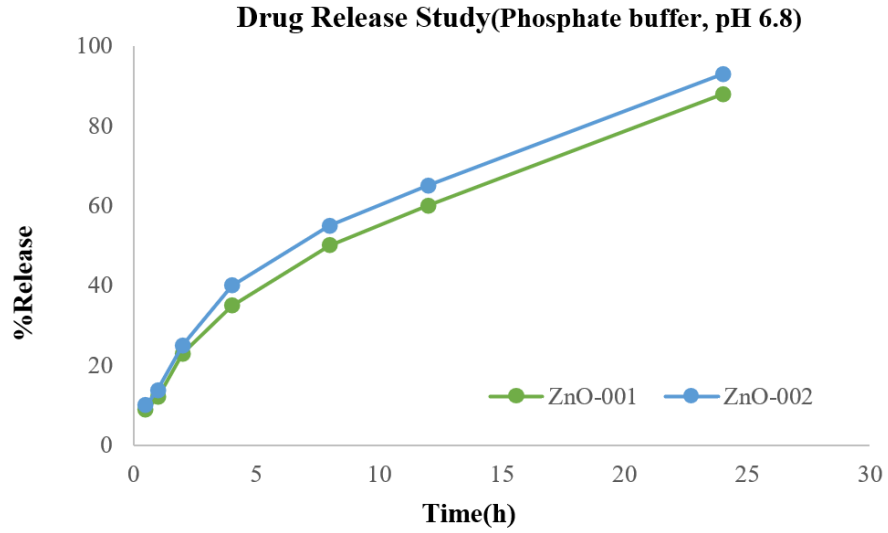

Figure 8. *In vitro* release profile study of Zn-loaded SLNs in Phosphate buffer, pH 6.8.

OES selectively quantifies free Zn^{2+} in solution and does not detect intact ZnO nanoparticles, the reported profiles strictly represent ionic zinc release Convention, 2019.

To elucidate the release mechanism, the data were fitted to various kinetic models, including Higuchi, Korsmeyer–Peppas, and first-order models. Among these, the Higuchi model exhibited the best correlation, suggesting that drug release was predominantly governed by diffusion through the lipid matrix Higuchi, 1963. The regression coefficients (R^2 values) for all models are summarized in Table 4, confirming the superior fit of the Higuchi and Korsmeyer–Peppas models. This interpretation is further supported by the linear relationship observed between cumulative release and the square root of time. Furthermore, the release exponent values ($n \approx 0.48 - 0.52$) derived from the Korsmeyer–Peppas model indicate a Fickian diffusion mechanism Korsmeyer et al., 1983. This implies that the release process was primarily controlled by molecular dif-

Table 3. *In vitro* cumulative release of ZnO-SLNs (ZnO-001, ZnO-002) under gastric (pH 1.2) and intestinal (pH 6.8) conditions.

Time (h)	ZnO-001 (0.1 N HCl, pH 1.2)	ZnO-002 (0.1 N HCl, pH 1.2)	ZnO-001 (Phosphate buffer, pH 6.8)	ZnO-002 (Phosphate buffer, pH 6.8)
0.5	5.0	6.0	9.0	10.0
1.0	8.0	10.0	12.0	14.0
2.0	18.0	22.0	23.0	25.0
4.0	25.0	35.0	35.0	40.0
8.0	40.0	50.0	50.0	55.0
12.0	51.0	60.0	60.0	65.0
24.0	80.0	85.0	88.0	93.0

SLN: Solid lipid nanoparticle; ZnO: Zinc Oxide; Zn: Zinc. Data represent mean values (n = 3) for ZnO-001 and ZnO-002 formulations at different time intervals up to 24 h.

Table 4. Release kinetics model fitting of ZnO-SLNs (ZnO-001, ZnO-002).

Formulation code	Zero-order (R^2)	First-order (R^2)	Higuchi (R^2)	Korsmeyer–Peppas (R^2)	Best-fit model(s)
ZnO-001 (0.1 N HCl, pH 1.2)	0.968	0.987	0.996	0.998	Korsmeyer–Peppas/Higuchi
ZnO-002 (0.1 N HCl, pH 1.2)	0.917	0.986	0.994	0.998	Korsmeyer–Peppas/Higuchi
ZnO-001 (Phosphate buffer, pH 6.8)	0.941	0.975	0.998	0.998	Higuchi/Korsmeyer–Peppas
ZnO-002 (Phosphate buffer, pH 6.8)	0.926	0.973	0.995	0.998	Higuchi/Korsmeyer–Peppas

ZnO: Zinc oxide; Zn: Zinc.

fusion, with minimal contribution from matrix swelling or erosion, thereby ensuring a predictable and sustained drug release profile.

Release kinetics model fitting of ZnO-loaded solid lipid nanoparticles (SLNs) under simulated gastric (pH 1.2) and intestinal (pH 6.8) conditions. Regression coefficients (R^2) are shown for zero-order, first-order, Higuchi, and Korsmeyer–Peppas models. Best-fit models are indicated for each formulation.

3.8 Drug loading efficiency and encapsulation performance

The encapsulation efficiency (EE%) represents the percentage of drug successfully entrapped within the nanoparticles (NPs) and was determined using equation (1):

$$EE\% = \frac{\text{Total drug conc.-supernatant drug conc.}}{\text{Total drug conc.}} \times 100 \quad (1)$$

The ZnO-SLN formulations demonstrated consistently high encapsulation efficiency. ZnO-001 (0.15 mM) achieved around 80%, while ZnO-002 (0.30 mM) reached nearly 90% (Table 5). As expected, drug loading increased with higher ZnO input, with ZnO-002 showing superior loading while maintaining good stability and a narrow size distribution. These findings confirm the system's effectiveness in incorporating ZnO and highlight its potential for oral delivery Mehnert and Mäder, 2001.

Table 5. EE% of zinc in the structure of prepared SLNs.

Formulation name	EE (%)
SLN	-
ZnO-001	80 ± 2.0%
ZnO-002	90 ± 3.0%

EE: Encapsulation efficiency; ZnO: Zinc oxide; Zn: Zinc; SD: Standard deviation. The results are expressed as means ± SDs (n = 3).

3.9 Cytotoxicity assay (MTT)

The cytotoxicity of the formulations ZnO-001 and ZnO-002 was assessed using the MTT assay at 24, 48, and 72-hour intervals (Table 6 and 7; Fig. 9–11(11a, 11b, 11c, 11d)). Notably, cell viability consistently remained at or above 100% compared to untreated controls across all time points, indicating excellent cytocompatibility. These results demonstrate the absence of cytotoxic effects and underscore the suitability of this SLN system for oral zinc delivery. Furthermore, the observed biocompatibility aligns well with previous studies on lipid-based nanocarriers, further supporting the potential of these formulations for safe biomedical applications Moezzi et al., 2012.

Statistical analysis of the cytotoxicity data was performed using one-way ANOVA followed by Tukey's post hoc test. All experiments were conducted in six replicates (n = 6), and data are expressed as mean ± standard deviation (SD). A statistically significant increase in cell viability was observed with increasing concentrations of ZnO-SLNs. The following p-values were obtained: $p < 0.05$ for comparisons at 24 h (250–500 µg/mL), $p < 0.01$ for comparisons at 48 h (125–500 µg/mL), and $p < 0.001$ for comparisons at 72 h (62.5–500 µg/mL). These results confirm the excellent cytocompatibility of both ZnO-001 and ZnO-002 formulations across all tested concentrations and time points.

While AGS cells were used to assess biocompatibility in this study, it is important to note that they represent gastric epithelial cells rather than intestinal tissue. This presents a limitation in evaluating the full potential of the formulation for oral delivery. To address this, future studies are recommended to incorporate intestinal cell lines such as Caco-2 or HT-29, which more accurately mimic the absorption and transport mechanisms of the human intestinal epithelium. Such models would provide deeper insight into the permeability and uptake behaviour of ZnO-SLNs across the gastrointestinal barrier.

Although the formulations exhibited excellent biocompatibility and sustained release profiles, it should be noted that intestinal absorption was not directly assessed. Future studies employing intestinal cell models are warranted to confirm the oral uptake potential of ZnO-SLNs. The cytocompatibility results obtained in this study are consistent with previous reports on the oral safety of ZnO nanoparticles and SLN-based systems, which have demonstrated minimal toxicity and favourable gastrointestinal tolerance Moezzi et al., 2012; Mukherjee et al., 2009; Pignatello et al., 2018.

3.10 Antimicrobial activity assessment

The antimicrobial potential of the ZnO-002 was systematically evaluated by the disk diffusion method (Table 8, figure 12). The formulation exhibited a clear concentration-dependent enhancement in antibacterial activity, as evidenced by progressive enlargement of the inhibition zones,

Table 6. Cytotoxicity assay of the prepared ZnO-001 formulation after 24, 48, and 72 hrs.

Concentration (µg/mL)	Control	15.625	31.25	62.5	125	250	500
Cell viability after 24 h	100	114.65	110.5	106.12	104.5	101	97
SD (n = 6)	3.5	4.8	5	6	6.2	5.8	7
Cell viability after 48 h	100	112.3	108.2	105.6	105.1	103	99.5
SD (n = 6)	3	5.3	6.1	4.8	6.2	5	5.5
Cell viability after 72 h	100	111.5	107.8	105	104.8	104	100
SD (n = 6)	2.8	6.4	6	5.8	5.3	4.8	5

Table 7. Cytotoxicity assay of the prepared ZnO-002 formulation after 24, 48, and 72 hrs.

Concentration (µg/mL)	Control	15.625	31.25	62.5	125	250	500
Cell viability after 24 h	100	114.65	110.5	106.12	104.5	101	97
SD (n = 6)	3.5	4.8	5	6	6.2	5.8	7
Cell viability after 48 h	100	111.8	108.2	105.6	105.1	103	99.5
SD (n = 6)	3	5.3	5.7	4.8	6.2	5	5.5
Cell viability after 72 h	100	110.6	106.8	105	104.8	104	100
SD (n = 6)	2.8	6.1	4.9	5.8	5.3	4.8	5.1

ZnO: Zinc oxide; Zn: Zinc; SD: Standard deviation. The results are expressed as means ± SDs (n = 3).
The results are presented as means ± SDs (n = 6).

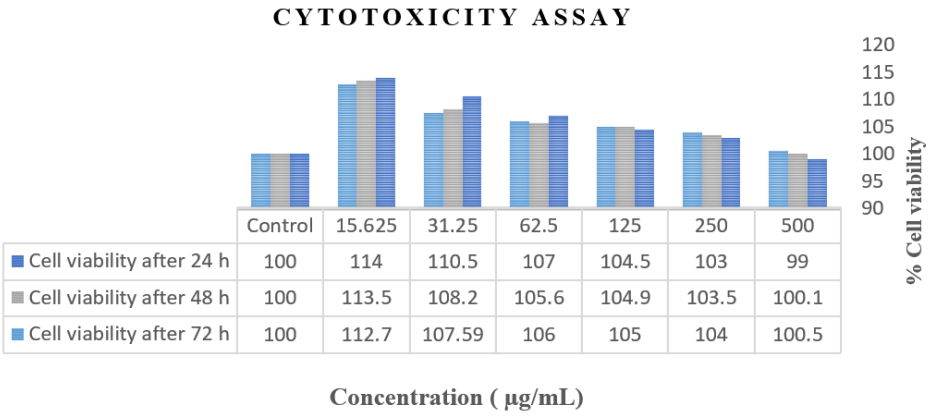

Figure 9. SLN cytotoxicity assay: Relative cell viability for ZnO-001 formulation after 24, 48, and 72 hrs.

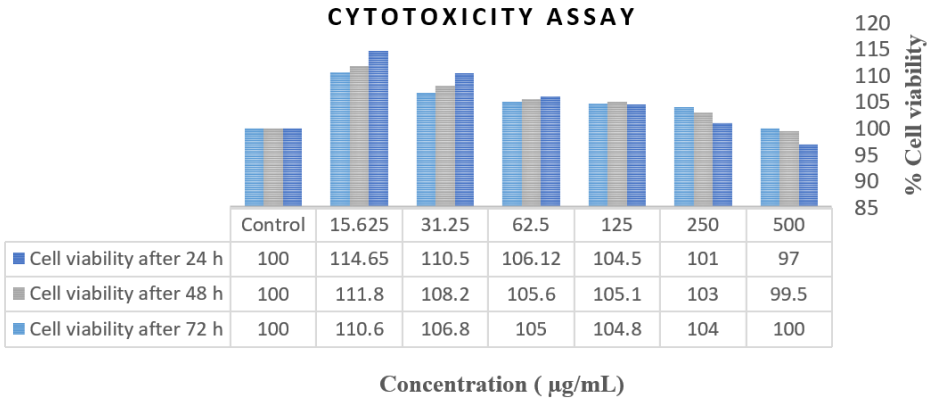

Figure 10. SLN cytotoxicity assay: Relative cell viability for ZnO-002 formulation after 24, 48, and 72 hrs.

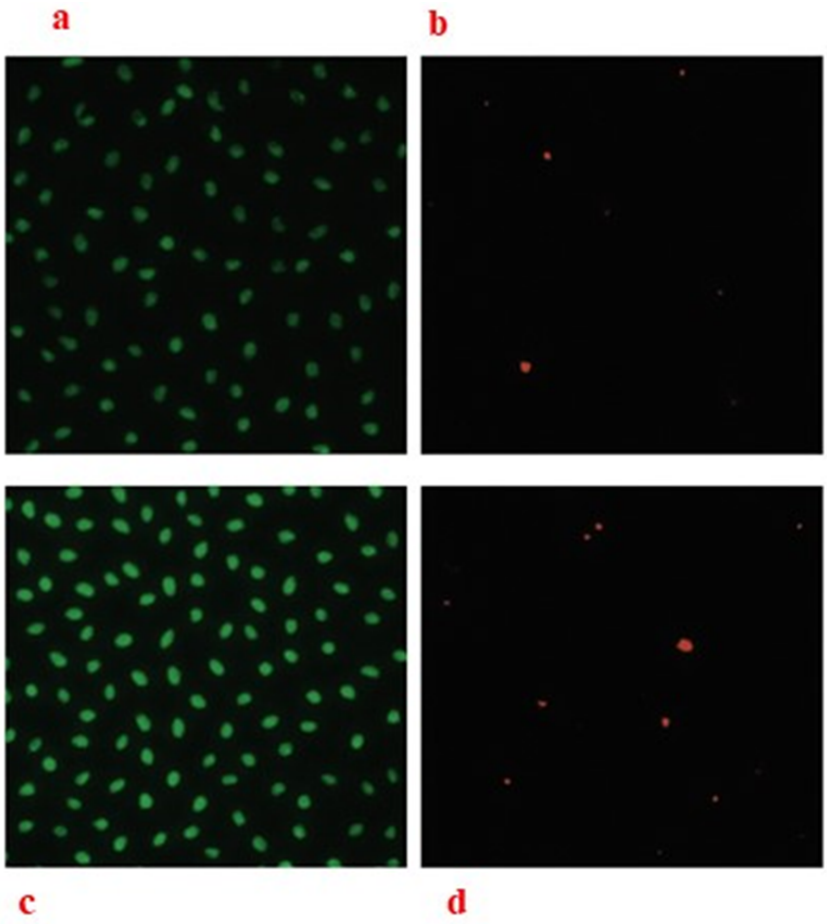

Figure 11. SLN cytotoxicity assay: Fluorescence microscopy images showing live cells (green) and dead cells (red). (a) and (b) correspond to ZnO-001 formulation; (c) and (d) correspond to ZnO-002 formulation.

with the maximum effect observed at 1000 µg/mL. When benchmarked against ampicillin, ZnO-002 demonstrated comparable, and in certain cases superior, inhibitory activity, underscoring its therapeutic relevance. Notably, the formulation was effective against both Gram-positive (*S. aureus*, *B. cereus*) and Gram-negative (*E. coli*, *P. aeruginosa*) strains, confirming its broad-spectrum antibacterial profile. The pronounced activity of ZnO-002 can be ascribed to its higher payload capacity and superior encapsulation efficiency, which likely promote sustained release and enhanced bioavailability of the active component. These attributes, combined with the reproducibility of the disk diffu-

Table 8. Antibacterial activity of ZnO-002 SLNs: Inhibition zones (disk diffusion).

Bacterial strain	Concentration (μg/mL)	Inhibition zone diameter (mm)	Ampicillin (mm)
P. aeruginosa (ATCC 27853)	1000	12	15
	500	11	
	250	10	
S. aureus (ATCC 29213)	1000	15	10
	500	12	
	250	10	
E. coli (ATCC 25922)	1000	12	7
	500	11	
	250	10	
B. cereus (ATCC 14579)	1000	15	7
	500	12	
	250	10	

ZnO: Zinc oxide; Zn: Zinc.

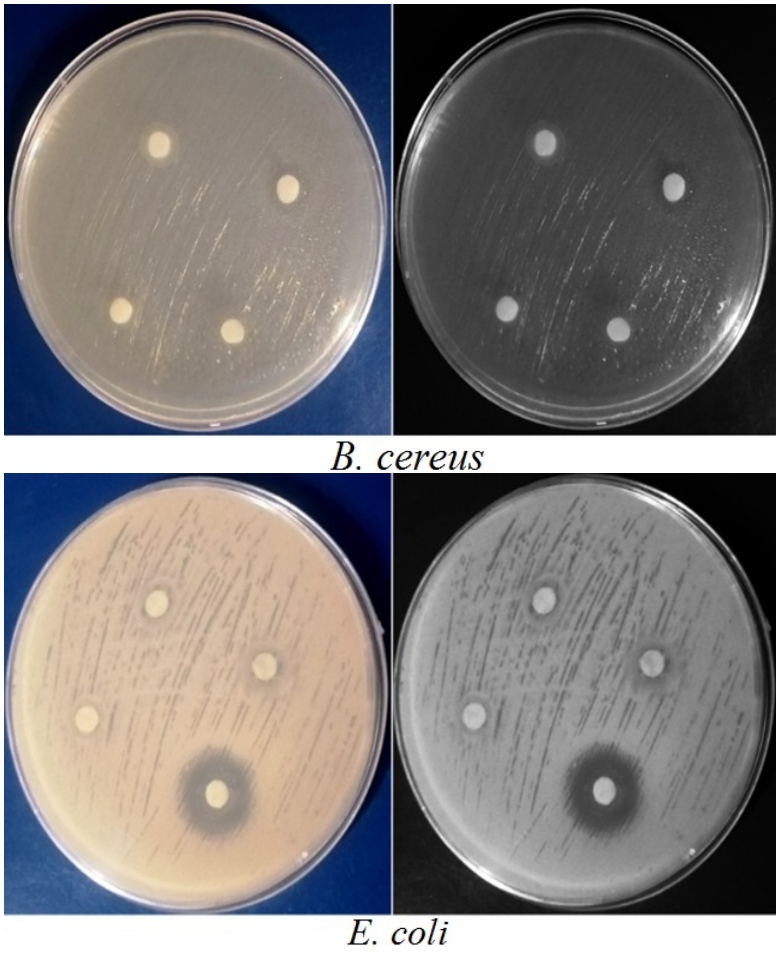

Figure 12. Antibacterial disk diffusion assay of ZnO-002: Zone of inhibition visualisation.

sion assay, provide strong evidence that ZnO-002 represent a promising nanocarrier system with significant potential for antimicrobial applications Raghupathi et al., 2011.

Table 8 Inhibition zone diameters (mm) of ZnO-002 SLNs against Gram-negative (*P. aeruginosa*, *E. coli*) and Gram-positive (*S. aureus*, *B. cereus*) bacteria at different concentrations. Ampicillin was used as the antibiotic control.

Table 9 Minimum inhibitory concentration (MIC) and minimum bactericidal concentration (MBC) of ZnO-002 SLNs against Gram-negative (*P. aeruginosa*, *E. coli*) and Gram-positive (*S. aureus*, *B. cereus*) bacteria, determined by broth microdilution. Values are expressed as mean ± SD (n = 3). Ampicillin was used as the antibiotic control.

3.11 Evaluation of accelerated stability

As summarized in Table 10, both formulations exhibited excellent stability under accelerated storage conditions (40 ± 2 °C, 75 ± 5% relative humidity) over 6 months. A negligible increase in particle size was observed, with final mean diameters remaining well below 110 nm. The PDI values, while showing a slight increase, consistently remained below 0.65, confirming the maintenance of a narrow size distribution. A modest shift in zeta potential towards neutral values was attributed to surfactant reorganization, yet the high absolute values ($\leq +17.6$ mV) ensured sufficient electrostatic repulsion to prevent aggregation.

Encapsulation efficiency (EE%) demonstrated remarkable

Table 9. Antibacterial activity of ZnO-002 SLNs: MIC and MBC values (broth microdilution).

Formulation	Bacterial strain	MIC (μg/mL)	MBC (μg/mL)	Ampicillin (μg/mL)
ZnO-002	*P. aeruginosa* (ATCC 27853)	64 ± 5	128 ± 8	8
	S. aureus (ATCC 29213)	32 ± 4	64 ± 6	4
	E. coli (ATCC 25922)	64 ± 5	128 ± 8	8
	B. cereus (ATCC 14579)	32 ± 4	64 ± 6	4

ZnO: Zinc oxide; Zn: Zinc.

Table 10. Physical stability data of optimized ZnO-SLN formulations under accelerated storage conditions (40 ± 2 °C, 75 ± 5% RH) for 6 months (n = 3, mean ± SD).

Formulation code	Time (Month)	Size (nm)	PDI	Zeta potential (mV)	EE (%)
ZnO-001 (coated, after lyophilization)	0	99.4 ± 3.5	0.545 ± 0.15	+28.4 ± 7.07	80.0 ± 2.0
	3	100.1 ± 4.2	0.561 ± 0.08	+20.5 ± 5.4	79.5 ± 2.8
	6	100.7 ± 5.5	0.583 ± 0.09	+17.6 ± 5.3	78.1 ± 3.2
ZnO-002 (coated, after lyophilization)	0	91.2 ± 2.8	0.582 ± 0.15	+32.1 ± 7.76	90.0 ± 3.0
	3	92.8 ± 3.7	0.595 ± 0.10	+24.5 ± 5.1	88.8 ± 2.5
	6	93.3 ± 4.9	0.614 ± 0.12	+20.0 ± 5.3	88.0 ± 3.5

PDI: Polydispersity index; SLN: Solid lipid nanoparticle; Zn: Zinc; SD: Standard deviation, EE: Encapsulation efficiency. The values are expressed as means ± SDs (n = 3).

retention, with a loss of less than 2.5%, underscoring the lipid matrix's robustness in retaining the payload. These findings confirm the outstanding colloidal and physical stability of the formulations, in line with previous reports on the stability of SLN systems Mehnert and Mäder, 2001; Zielińska et al., 2018; Zielińska et al., 2020; Sastri et al., 2020. Collectively, the results affirm the suitability of these formulations for long-term storage and highlight their potential for commercial application.

4. Conclusion

This study successfully developed and characterized two zinc oxide solid lipid nanoparticle (ZnO–SLN) systems, ZnO-001 and ZnO-002, both of which exhibited favorable physicochemical properties, stability after lyophilization, and promising encapsulation efficiency. Among these, ZnO-002 demonstrated a higher drug payload and superior encapsulation efficiency, and was therefore selected for detailed antimicrobial evaluation. This formulation showed a clear concentration-dependent antibacterial effect, with inhibition zones comparable to or even greater than those of ampicillin against selected Gram-positive and Gram-negative bacterial strains. Furthermore, drug release studies performed at intestinal pH (6.8) support the potential of ZnO–SLNs for oral delivery applications.

Despite these promising findings, certain limitations should be acknowledged. Intestinal absorption was not directly assessed in this study, and cytotoxicity evaluation was restricted to AGS gastric epithelial cells. Future investigations should therefore incorporate intestinal cell models, such as Caco-2 or HT-29, to better simulate oral uptake. Moreover, although encapsulation efficiency was quantified using ICP-OES—a highly sensitive and reliable technique for inorganic nanomaterials—validation using complementary analytical methods would further enhance the robustness of the findings.

In conclusion, both ZnO–SLN formulations exhibit strong potential as orally deliverable nanocarrier systems, with ZnO-002 demonstrating superior antimicrobial performance. Further in vivo and mechanistic studies are warranted to confirm their therapeutic efficacy and absorption characteristics, paving the way for their potential biomedical applications.

Authors contributions
Authors have contributed equally in preparing and writing the manuscript.

Availability of data and materials
The data that support the findings of this study are available from the corresponding author, upon reasonable request.

Conflict of interests
The authors declare that they have no known competing financial interests or personal relationships that could have appeared to influence the work reported in this paper.

References

Agnihotri S. A., Mallikarjuna N. N., Aminabhavi T. M. (2004) Recent advances on chitosan-based micro- and nanoparticles in drug delivery. *J Control Release* 100 (1): 5–28. DOI: https://doi.org/10.1016/j.jconrel.2004.08.010.

Allen L., Benoist B. de, Dary O., Hurrell R. (2006) Guidelines on food fortification with micronutrients. *World Health Organization*

Bernkop-Schnürch A., Dünnhaupt S. (2012) Chitosan-based drug delivery systems. *Eur J Pharm Biopharm* 81 (3): 463–469. DOI: https://doi.org/10.1016/j.ejpb.2012.04.007.

Black R. E. (2003) Trace element undernutrition: biology to interventions. *J Nutr* 133 (5 Suppl 1): 1485S–1489S. DOI: https://doi.org/10.1093/jn/133.5.1485S.

Brown K. H., Wuehler S. E., Peerson J. M. (2001) The importance of zinc in human nutrition and estimation of the global prevalence of zinc deficiency. *Food Nutr Bull* 22 (2): 113–125. DOI: https://doi.org/10.1177/156482650102200201.

Clinical, Institute Laboratory Standards (2015) Methods for dilution antimicrobial susceptibility tests for bacteria that grow aerobically; approved standard—tenth edition. *CLSI document M07-A10*

Convention The United States Pharmacopeial (2019) United States Pharmacopeia 42 – National Formulary 37 (USP 42–NF 37). *USP*

Date A. A., Hanes J., Ensign L. M. (2016) Nanoparticles for oral delivery: design, evaluation and state-of-the-art. *J Control Release* 240:504–526. DOI: https://doi.org/10.1016/j.jconrel.2016.06.016.

Ebrahimi H. A., Javadzadeh Y., Hamidi M., Jalali M. B. (2015) Repaglinide-loaded solid lipid nanoparticles: effect of using different surfactants/stabilizers on physicochemical properties of nanoparticles. *DARU J Pharm Sci* 23:46. DOI: https://doi.org/10.1186/s40199-015-0128-3.

Ekambaram P., Sathali A. A. H., Priyanka K. (2012) Solid lipid nanoparticles: a review. *Sci Revs Chem Commun* 2 (1): 80–102.

Espitia P. J. P., Soares N. F. F., Reis Coimbra J. S. dos, Andrade N. J. de, Cruz R. S., Medeiros E. A. A. (2012) Zinc oxide nanoparticles: synthesis, antimicrobial activity and food packaging applications. *Food Bioprocess Technol* 5 (5): 1447–1464. DOI: https://doi.org/10.1007/s11947-012-0797-6.

Food U.S., (FDA) Drug Administration (2024) Inactive Ingredient Database (IID). https://www.fda.gov/drugs/drug-approvals-and-databases/inactive-ingredients-database

Gasco M. R. (1997) Solid lipid nanospheres from warm microemulsions. *Pharm Technol Eur* 9:52–58.

Higuchi T. (1963) Mechanism of sustained-action medication. Theoretical analysis of rate of release of solid drugs dispersed in solid matrices. *J Pharm Sci* 52 (12): 1145–1149. DOI: https://doi.org/10.1002/jps.2600521210.

Hosseini S. M., Abbasalipourkabir R., Jalili C., Zarei L. (2020) Preparation of a nanoliposomal carrier for the oral delivery of zinc and the evaluation of its stability, cytotoxicity, and bioaccessibility. *J Food Sci* 85 (12): 4263–4271. DOI: https://doi.org/10.1111/1750-3841.15532.

Joseph J. J., Sangeetha D., Gomathi T. (2016) Sunitinib loaded chitosan nanoparticles formulation and its evaluation. *Int J Biol Macromol* 82:952–958. DOI: https://doi.org/10.1016/j.ijbiomac.2015.10.077.

King J. C. (2011) Zinc: an essential but elusive nutrient. *Am J Clin Nutr* 94 (2 Suppl): 679S–684S. DOI: https://doi.org/10.3945/ajcn.110.005744.

Korsmeyer R. W., Gurny R., Doelker E., Buri P., Peppas N. A. (1983) Mechanisms of solute release from porous hydrophilic polymers. *Int J Pharm* 15 (1): 25–35. DOI: https://doi.org/10.1016/0378-5173(83)90064-9.

Luo Y., Teng Z., Li Y., Wang Q. (2015) Solid lipid nanoparticles for oral drug delivery: chitosan coating improves stability, controlled delivery, mucoadhesion and cellular uptake. *Carbohydr Polym* 122:221–229. DOI: https://doi.org/10.1016/j.carbpol.2014.12.084.

Mahajan P. S., Mahajan K. B., Darekar A. B. (2015) A review on solid lipid nanoparticle (SLN): an advanced treatment modality. *Int J Pharm Sci Res* 6 (9): 3698–3712. DOI: https://doi.org/10.13040/IJPSR.0975-8232.6(9).3698-3712.

Mehnert W., Mäder K. (2001) Solid lipid nanoparticles: production, characterization and applications. *Adv Drug Deliv Rev* 47 (2-3): 165–196. DOI: https://doi.org/10.1016/S0169-409X(01)00105-3.

Mishra P. K., Mishra H., Ekielski A., Talegaonkar S., Vaidya B. (2017) Zinc oxide nanoparticles: a promising nanomaterial for biomedical applications. *Drug Discov Today* 22 (12): 1825–1834. DOI: https://doi.org/10.1016/j.drudis.2017.08.006.

Moezzi A., McDonagh A. M., Cortie M. B. (2012) Zinc oxide particles: synthesis, properties and applications. *Chem Eng J* 185–186:1–22. DOI: https://doi.org/10.1016/j.cej.2012.01.076.

Mohammed M. A., Syeda J. T. M., Wasan K. M., Wasan E. K. (2017) An overview of chitosan nanoparticles and its application in non-parenteral drug delivery. *Pharmaceutics* 9 (4): 53. DOI: https://doi.org/10.3390/pharmaceutics9040053.

Mukherjee S., Ray S., Thakur R. S. (2009) Solid lipid nanoparticles: a modern formulation approach in drug delivery system. *Indian J Pharm Sci* 71 (4): 349–358. DOI: https://doi.org/10.4103/0250-474X.57282.

Müller R. H., Eder K., Gohla S. (2000) Solid lipid nanoparticles (SLN) for controlled drug delivery: a review of the state of the art. *Eur J Pharm Biopharm* 50 (1): 161–177. DOI: https://doi.org/10.1016/S0939-6411(00)00087-4.

Müller R. H., Radtke M., Wissing S. A. (2002) Solid lipid nanoparticles (SLN) and nanostructured lipid carriers (NLC) in cosmetic and dermatological preparations. *Adv Drug Deliv Rev* 54 (Suppl 1): S131–S155. DOI: https://doi.org/10.1016/S0169-409X(02)00118-7.

Patel K. V., Nath M., Bhatt M. D., Dobriyal A. K., Bhatt D. (2020) Nanoformulation of zinc oxide and chitosan-zinc nano-bioformulation sustain oxidative stress and alter secondary metabolite profile in tobacco. *3 Biotech* 10 (11): 477. DOI: https://doi.org/10.1007/s13205-020-02469-x.

Patel R., Patel M., Patel K. (2014) Development and characterization of solid lipid nanoparticles for enhanced oral bioavailability of poorly water-soluble drugs. *J Pharm Investig* 44 (4): 287–302. DOI: https://doi.org/10.1007/s40005-014-0120-6.

Pignatello R., Leonardi A., Fuochi V., Petronio G. P., Greco A. S., Furneri P. M. (2018) A method for efficient loading of ciprofloxacin hydrochloride in cationic solid lipid nanoparticles: formulation and microbiological evaluation. *Nanomaterials (Basel)* 8 (5): 304. DOI: https://doi.org/10.3390/nano8050304.

Prasad A. S. (2008) Zinc in human health: effect of zinc on immune cells. *Curr Opin Clin Nutr Metab Care* 11 (6): 646–652. DOI: https://doi.org/10.1097/MCO.0b013e3283138ab4.

Program National Toxicology (2008) Toxicological profile for 1-Butanol. *Toxicol Ind Health* 24 (9): 597–606. DOI: https://doi.org/10.1177/0748233708098116.

Prokhorov E., Luna-Bárcenas J. G., Espinoza-González R., Rentería-Covarrubias N., González-González V., Hernández-Escobar C. A. et al. (2020) Chitosan-zinc oxide nanocomposites assessed by dielectric, conductivity, mechanical, and piezoelectric properties. *Polymers (Basel)* 12 (9): 1991. DOI: https://doi.org/10.3390/polym12091991.

PubChem (2024) 1-Butanol. National Center for Biotechnology Information. *PubChem Compound Summary for CID 263,* https://pubchem.ncbi.nlm.nih.gov/compound/1-Butanol

Raghupathi K. R., Koodali R. T., Manna A. C. (2011) Size-dependent bacterial growth inhibition and mechanism of antibacterial activity of zinc oxide nanoparticles. *Langmuir* 27 (7): 4020–4028. DOI: https://doi.org/10.1021/la104825u.

Salgueiro M. J., Zubillaga M. B., Lysionek A. E., Caro R. A., Weill R., Boccio J. R. (2002) The role of zinc in the growth and development of children. *Nutr Res* 22 (7): 1005–1015. DOI: https://doi.org/10.1016/S0271-5317(02)00418-8.

Sastri K. T., Radha G. V., Pidikiti S., Vajjhala P. (2020) Solid lipid nanoparticles: Preparation techniques, their characterization, and an update on recent studies. *J Appl Pharm Sci* 10 (6): 126–141. DOI: https://doi.org/10.7324/JAPS.2020.10617.

Scioli-Montoto S., Allemann E., Mattos A. C., Espina M., Souza J., García M. L. et al. (2020) Solid lipid nanoparticles for drug delivery: A review of the state of the art. *Front Mol Biosci* 7:587997. DOI: https://doi.org/10.3389/fmolb.2020.587997.

Selvaraj P., Kalimuthu A., Manjunathan N., Palaniswamy K., Kathirvel D., Rajamani R. et al. (2020) Synthesis and characterization of chitosan/zinc oxide nanocomposite for antibacterial activity onto cotton fabrics and dye degradation applications. *Int J Biol Macromol* 164:2779–2787. DOI: https://doi.org/10.1016/j.ijbiomac.2020.08.047.

Trivedi S. S., Chudasama R. K., Patel N. (2009) Effect of zinc supplementation in children with acute diarrhea: randomized double blind controlled trial. *Gastroenterol Res* 2 (3): 137–142. DOI: https://doi.org/10.4021/gr2009.06.1297.

Vigani B., Valentino C., Sandri G., Listro R., Fagiani F., Collina S. et al. (2021) A composite nanosystem as a potential tool for the local treatment of glioblastoma: chitosan-coated solid lipid nanoparticles embedded in electrospun nanofibers. *Polymers (Basel)* 13 (9): 1371. DOI: https://doi.org/10.3390/polym13091371.

Winter E., Pizzol C. D., Locatelli C., Creczynski-Pasa T. B. (2016) Development and evaluation of lipid nanoparticles for drug delivery: study of toxicity in vitro and in vivo. *J Nanosci Nanotechnol* 16 (2): 1321–1330. DOI: https://doi.org/10.1166/jnn.2016.11676.

Yanti D. D., Maryanti E. (2021) Green synthesis ZnO nanoparticles using rinds extract of *Sapindus rarak* DC. *J Sci Appl Technol* 5 (1): 198.

Zielińska A., Carretero C., Zieliński H., Souto E. B. (2020) Loading, release profile and accelerated stability assessment of monoterpenes-loaded solid lipid nanoparticles (SLN). *J Microencapsul* 37 (3): 211–221. DOI: https://doi.org/10.1080/10837450.2020.1744008.

Zielińska A., Nowak I., Makuch E., Wójcik M., Carretero C., Souto E. B. (2018) Optimization of citral-loaded solid lipid nanoparticles (SLN): factorial design and accelerated stability testing. *Int J Pharm* 553 (1–2): 428–440. DOI: https://doi.org/10.1016/j.ijpharm.2018.10.037.